

A Mixed-Finite Element Approach for Performance-Based Design of Rectangular Concrete-Filled Steel Tube (RCFT) Frames

Cenk Tort
Staff Engineer
Skidmore, Owings, & Merrill LLP
Chicago, USA
cenk.tort@som.com

Jerome F. Hajjar
Professor
University of Illinois at Urbana-Champaign
Urbana, USA
jfhajjar@uiuc.edu

ABSTRACT

A comprehensive computational model to simulate the nonlinear seismic response of composite frames with rectangular concrete-filled steel tube (RCFT) beam-columns and steel girders and braces is presented in this work. A three-dimensional fiber-based distributed plasticity mixed finite element formulation is introduced. The finite element formulation of RCFT beam-columns was derived with separate translational degrees-of-freedom (DOFs) defined for the concrete core and the steel tube to simulate the slip deformation that is typical for composite members. Cyclic constitutive relations were derived accounting for the interactions taking place between the steel tube and the concrete core including slip, confinement, and local buckling. A representative composite frame structure was analyzed under a suite of ground motion records and the demand imposed on the RCFT columns was quantified. A methodology based on the use of the damage function equations was proposed to evaluate the performance of RCFT members under seismic loads.

INTRODUCTION

Integrating the favorable characteristics of the steel tube and the concrete core in RCFTs provides an efficient design alternative for beam-columns in the lateral load resistance systems of low, moderate, and high rise structures. The advantages offered by RCFTs such as high strength, stiffness, ductility, and economy have long been recognized, which resulted in extensive experimental and computational research studies toward understanding their behavior and developing reliable design methods. The experimental database studies by [Aho and Leon 1997], [Tort and Hajjar 2004], [Kim 2005], and [Gourley et al. 2008] show that there exist significant experimental data in the literature that indicate the superior performance of RCFTs under static and quasi-static loading conditions. In recent experimental work on large scale multistory RCFT frames under dynamic loading, RCFT frames were found to exhibit a stable response under earthquake loading with large energy dissipation and low strength deterioration

[Tsai et al. 2003], [Herrera 2005]. The information gained from this prior research on composite beam-columns resulted in the development of several new provisions in the 2005 AISC *Specification for Structural Steel Buildings* [AISC 2005]. Leon et al. [2007] utilized the available experimental research to update the design of composite columns, where the composite interaction is taken into account more accurately through improved quantification of the concrete contribution to the flexural response. This approach helps to reduce the over-conservatism introduced by neglecting the contribution of concrete [Choi et al., 2006]. In addition, Leon et al. [2007] also recommended increasing the slenderness limit of the steel tube against local buckling. Despite the increasing number of available experimental tests and the improvement in the worldwide design specifications for non-seismic applications, guidance on earthquake resistance design of composite CFT columns still remains limited.

The quantification of seismic demand and capacity is vital in developing performance-based seismic resistant design methodologies. This is often achieved through nonlinear time-history analysis of frame structures for a range of hazard levels [Yun et al., 2002]. In this research study, a 3D beam finite element model was derived based on mixed finite element principles (building on prior research on displacement-based formulations [Schiller and Hajjar 1998]) to conduct nonlinear time history analysis of frame structures with RCFT members and steel columns. The model was calibrated and verified with respect to experimental specimens available in the literature. A representative RCFT frame was then analyzed under a suite of earthquake records and a methodology was proposed to evaluate the performance of the RCFT members utilizing the nonlinear time history analysis results.

FINITE ELEMENT FORMULATION

Mixed finite element principles were adopted to derive a 3D 18 DOF RCFT beam-column element. The 6 DOFs added to the standard 12 DOF beam formulation were defined to quantify the differential movement between the steel tube and the concrete core [Hajjar et al. 1998]. A two-field form of mixed finite element methods was used, where displacements and internal element forces are interpolated independently of each other. The element stiffness and internal forces were derived by considering only the deformational DOFs. The effect of rigid body modes was included in the formulation while calculating the quantities with respect to the global coordinates. Cubic Hermitian shape functions were defined for the transverse displacements while the axial deformations were represented via quadratic shape functions. The bending moment distribution was assumed to be linear. However, the second-order moments due to the $P-\delta$ effect, which are obtained by multiplying the axial forces and transverse deformations, were added to the linear distribution of bending moments [Alemdar and White 2005]. Interpolating the element internal forces allows satisfying the element equilibrium exactly, which helps achieving good coarse mesh accuracy compared to displacement-based formulations. In addition, it alleviates the numerical problems in displacement-based formulations due to concrete cracking while ensuring element equilibrium [Schiller and Hajjar 1998]. The mixed finite element formulation also allowed quantification of slip based on the difference in the assumed axial deformation fields for the concrete core and the steel tube.

The derivation of the formulation starts by expressing the equilibrium, compatibility, and cross-section equilibrium equations in their integral forms as given in Equations 1, 2 and 3. An Updated-Lagrangian formulation was utilized, where all the variables were defined with respect to the last converged configuration. In Equations 1 through 3, both superscripts and subscripts located to the left of a symbol refer to two configurations of interest. C1 represents the last converged state and C2 is the current state of the element body. A left superscript designates the configuration in which the quantity is measured. If a left superscript is omitted, the quantity

is considered as an increment between C1 and C2 or between the current and the next C2 configuration (e.g., during an iteration process). The terms in bold represent either matrix or vector quantities while the non-bold terms represent scalar quantities. The equilibrium equation defines the balance between the work done by externally applied loads and internal forces. A distinct feature of the formulation with respect to the composite action is that the effect of slip was accounted for by adding an additional term to the equilibrium equation for the slip deformation. The compatibility equation represents the balance between cross-section strains ($\hat{\mathbf{d}}$, e.g., axial strain, curvature) from the interpolated deformation fields and the cross-section strains (\mathbf{d}) corresponding to the interpolated forces obtained by multiplying the inverse of the cross-section rigidity by the interpolated cross-section forces. The kinematic relations assumed in this formulation were a Green-Lagrange axial strain measure and curvatures being the second derivative of the transverse deformations. The torsional response was taken as linear. The axial strains and curvatures were defined separately for the steel tube and the concrete as part of the slip formulation. The cross-section equilibrium defines the balance between the interpolated cross-section forces (\mathbf{D} , e.g., axial forces, bending moment) and the cross-section forces (\mathbf{D}_Σ) obtained from integration of stresses of the steel and concrete material fibers over the RCFT cross-section. The cross-sectional forces defined for the RCFT members were axial forces and bending moments introduced for the steel tube and the concrete core separately.

$$(1) \quad \int_0^{1L} \delta_1^2 \hat{\mathbf{d}}^T \times_1^2 \mathbf{D} \times d^1 x + \int_0^{1L} \delta_1^2 \hat{\mathbf{d}}_{sc}^T \times_1^2 \mathbf{D}_{sc} \times d^1 I + \int_{1V^c}^1 \rho^c \times_1^2 \ddot{\mathbf{u}}^c \times \delta_1^2 \mathbf{u}^c \times d^1 V^c + \int_{1V^s}^1 \rho^s \times_1^2 \ddot{\mathbf{u}}^s \times \delta_1^2 \mathbf{u}^s \times d^1 V^s + \int_{1V^c}^1 \mu^c \times_1^2 \dot{\mathbf{u}}^c \times \delta_1^2 \mathbf{u}^c \times d^1 V^c + \int_{1V^s}^1 \mu^s \times_1^2 \dot{\mathbf{u}}^s \times \delta_1^2 \mathbf{u}^s \times d^1 V^s - \delta_1^2 \mathbf{q}^T \times_1^2 \mathbf{Q}_{ext} = 0$$

$$(2) \quad \int_0^{1L} \delta_1^2 \mathbf{D}^T \times (\hat{\mathbf{d}} - \mathbf{d}) \times d^1 x = 0$$

$$(3) \quad \mathbf{D}_\Sigma - \mathbf{D} = 0$$

Linearization of Equations 1 through 3 with respect to their state variables results in the expressions for the element stiffness, mass, damping and internal forces. A non-iterative internal force calculation procedure was adopted, where the unbalances of the equilibrium and compatibility equations are eliminated through Newton-Raphson iterations conducted at the global level. The details of the formulation with the internal force calculation procedure can be found in [Tort and Hajjar 2007]. [Tort and Hajjar 2007] also developed a steel beam-column element following mixed finite element formulation to model girders in a composite frame.

MATERIAL CONSTITUTIVE RELATIONS

In the current formulation, the finite element was divided into several cross-sections along its length. Each cross-section was further subdivided into individual steel and concrete fibers, which were associated with a constitutive relation. Throughout the analysis, the nonlinearity occurring at the steel and concrete fibers was monitored and the nonlinearity was first passed to the cross-section level and then to the element level as the area and length integrations are performed, respectively while calculating the internal element forces. The fiber-based distributed plasticity approach to model nonlinearity was preferred compared to concentrated

plasticity formulations since detailed information on the damage state of the structure (e.g., concrete cracking, steel yielding) can be obtained, which is important in performance-based design for defining the performance objectives.

The concrete constitutive relations were adopted from [Chang and Mander 1994]. Three different curves were introduced defining the stress-strain response as shown in Figure 1. The envelope curves represented the backbones of the hysteretic response in tension and compression. The compression envelope curve was derived based on experimental data available in the literature on axially loaded RCFT column tests. It was assumed that the concrete core in compression behaves as plain concrete until the attainment of the peak strength. A linear strength degradation region with a slope of K_c initiates once the peak strength is reached. The extent of strength degradation depends on the degree of confinement provided by the steel tube and at high strain levels, the compressive stresses do not drop below a constant value defined as f_{rc} . Therefore, the slope of the strength degradation region and the constant stress level were correlated to the slenderness parameter of the steel tube as shown Equation 4. The envelope curve in tension was taken as similar to plain concrete. The connecting curves define the relation for strain histories ranging between the envelope curves. The transition curves provide the rules to shift from one connecting to the other going in opposite direction. The model by [Chang and Mander 1994] was augmented for RCFT members by defining new rules to increase its comprehensiveness under random cyclic loading histories. For example, as shown in Figure 1, a new rule was introduced if unloading takes place between the latest unloading point and the target point on the envelope curve.

$$(4a) \quad K_c = -332.75 \times R \times f'_c + 9.60 \times f'_c$$

$$(4b) \quad \frac{f_{rc}}{f'_c} = 0.32 \times R^{-0.5}$$

where: $R = \frac{D}{t} \times \sqrt{\frac{f_y}{E_s}} \times \frac{f'_c}{f_y}$

The constitutive model of the steel tube was adopted from [Mizuno et al. 1991], where the stress-strain response was traced based on evolution of loading and bounding surfaces. The loading surface defines the initiation of inelasticity while the bounding surface represents the limiting stress state attained by the material. The model accounts for typical characteristics of the steel such as Bauschinger effect, strain hardening, decreasing elastic zone etc. However, it was originally developed for hot-rolled steel. Since the focus of this research is study is on RCFT members with cold-formed steel sections, the model by [Mizuno et al. 1991] was modified to account for typical features of cold-formed tubes and also the composite interaction between the steel tube and the concrete core. Residual strain values were calibrated for the corner and flat regions of the steel tube from coupon tests available in the literature so that the premature yielding of the cold-formed steel tube can be captured. The calibrated values of initial strains were obtained as 0.0006 and 0.0004, for the corner and flat regions, respectively. In addition, the yield strength of the steel tube was assumed to be larger in the corner regions due to the effect cold forming and the ratio of the yield strength of the steel tube in corner regions to that of the flat regions was taken as 1.1 based on the coupon test results in the literature. The strain level at initiation of local buckling (ϵ_{lbf}) was calibrated from axially loaded RCFT column tests. Following local buckling, a linear strength degradation was assumed until a constant stress region is attained. The slope of the strength degradation region (K_s) and the constant stress level at high strains (f_{rs}) shown in Figure 2 were also calibrated with respect to axially loaded

RCFT column tests from the literature. In addition, it was assumed that local buckling also causes a reduction in the radius of the bounding surface ($\bar{\kappa}$) from its initial value ($\bar{\kappa}_o$). The rate of reduction of the radius of the bounding surface (γ_{cc}) was correlated to the plastic work done (W^p) during cyclic loading and it is calibrated to the cyclically loaded tests of RCFT members. Key equations of the steel model are given below:

$$(5a) \quad \frac{\varepsilon_{lbf}}{\varepsilon_y} = 3.14 \times \left(\frac{D}{t} \sqrt{\frac{f_y}{E_s}} \right)^{-1.48}$$

$$(5b) \quad K_s = 0, (D/t) \times (f_y / E_s) \leq 0.08$$

$$K_s = -644304.39 \times (D/t) \times (f_y / E_s) + 51544.35, (D/t) \times (f_y / E_s) \geq 0.08$$

$$(5c) \quad \frac{f_{rs}}{f_y} = 1 \text{ for } (D/t) \times (f_y / E_s) \leq 0.08$$

$$\frac{f_{rs}}{f_y} = -7.31 \times (D/t) \times (f_y / E_s) + 1.58 \text{ for } (D/t) \times (f_y / E_s) \geq 0.08$$

$$(5d) \quad \bar{\kappa} = (-\gamma_{cc} \times W^p + 1) \times \bar{\kappa}_o$$

$$(5d) \quad \gamma_{cc} = 0.0345 \quad (D/t) \times \sqrt{f_y / E_s} < 0.92$$

$$(5e) \quad \gamma_{cc} = 0.196 \times (D/t) \times \sqrt{f_y / E_s} - 0.146 \quad 0.92 \leq (D/t) \times \sqrt{f_y / E_s} \leq 1.45$$

$$(5f) \quad \gamma_{cc} = 0.138 \quad (D/t) \times \sqrt{f_y / E_s} > 1.45$$

VERIFICATION STUDIES OF THE MODEL

The finite element formulation along with constitutive relations were implemented in [OpenSees 2001]. The accuracy of the formulation and the constitutive relations were tested against numerous specimens from the literature. The RCFT beam-column specimens by [Cederwall et al. 1991] and by [Varma et al. 2002] were analyzed under eccentrically applied axial load and constant axial load and increasing bending moment, respectively. For both of the specimens, 2 elements per member with 4 integration points were defined and a displacement-controlled solution algorithm was applied. The capacity of the specimens exhibited excellent correlation with computational results as shown in Figure 3. The failure of Specimen 1 by [Cederwall et al. 1991] was governed by flexural buckling, which is accurately captured by the analysis with close agreement with the pre-peak and post-peak regions of the load-deformation response. Specimen BC32-80-40 by [Varma et al. 2002] underwent significant softening response due to the large axial load ratio and the softening behavior as a result of concrete crushing and local buckling of the steel tube, which is also captured successfully by the proposed model. The second verification study involved analysis of RCFT members under quasi-static cyclic loading, where the RCFT member, CIIS3-3 by [Tomii and Sakino 1979] and SR6A4C by [Inai et al. 2004], are tested under constant axial load and cyclic shear loading, putting the members into double curvature. The computational model and experimental results showed excellent

agreement as can be seen in Figure 4. The shear and moment capacity, and the loading and unloading stiffnesses were estimated by the computational model accurately.

PERFORMANCE-BASED DESIGN METHODOLOGY

A typical 3-story RCFT structure was analyzed under a suite of far field earthquake records. The seismic response parameters were documented and a methodology to evaluate the performance of the RCFT members was presented based on the prior work by [Tort and Hajjar 2004].

The RCFT structure was assumed to be located in Los Angeles and NEHRP Site Class D soil conditions were considered. As defined in Figure 5, the structure has 4 bays of RCFT columns and steel girders [LaFore and Hajjar 2005]. The mass at each story was assumed to be lumped at the joint locations and 2% damping ratio was assumed. A total of 12 far-field ground motion records were used and they were selected to minimize the discrepancy between the spectral acceleration values at the first mode period of the structure with respect to design spectrum and the median spectrum so that large scale factors are avoided and a more accurate estimation of the nonlinear response with reduced biases can be obtained [Tort and Hajjar 2007]. The scaling of the records was done based on the first mode period of the structure.

The nonlinear time-history analysis of the structure for the selected earthquake records was conducted following the application of the factored gravity loading. Table 1 summarizes the seismic response parameters obtained from the analysis results for 2%50 hazard level. The mean (μ) and 84 percentile ($\mu + \sigma$) values of maximum and minimum of roof drift (Δ_r) as a percentage of the height of the structure (h_r), inter-story drift ratio (IDR), and story shear (V_r) are shown. The maximum and minimum of values of IDR and V_r were found to be in the 1st story of the structure. It can be seen in Table 1 that the μ and $\mu + \sigma$ values of the seismic response parameters do not significantly deviate from each other, indicating nearly uniform demand levels over the selected earthquake records.

Tort and Hajjar [2004] proposed a deformation-based damage function (\hat{D}) to quantify the damage experienced by RCFT members as given in Equation 6. The value of the damage functions indicating the occurrence of local damage states (e.g., concrete cracking, concrete crushing, steel yielding, etc.) were obtained from the available experiments in the literature and equations were derived in terms of geometric and material properties of RCFT members to estimate those damage function values. Tort and Hajjar [2004] also correlated the ranges of the damage function to the performance-levels e.g., Immediate Occupancy, Life Safety etc.

$$(6) \quad \hat{D} = \frac{d_{curr}}{d_o}$$

The time-history analysis results were utilized to quantify the deformation-based damage function values of the RCFT columns of the studied frame structure. First, static push-over analysis of the structure was conducted, where d_o of the columns were obtained from the chord rotation (R) vs. moment response extracted for each RCFT column from the push-over analysis, where R was calculated as the ratio of lateral displacement to the element length. d_o was assumed to be the R value attained when the stiffness of the RCFT column becomes 10% of its initial value. As shown In Figure 6, moment vs. R response from the static push-over analysis and time history analysis are superimposed for the windward interior column at the first story of the frame. d_{curr} was obtained from the time history analysis results as the mean

maximum R experienced during the ground motions. \hat{D} was calculated as the ratio of d_{curr} and d_o . It was found that mean \hat{D} values ranges from 0.41 to 1.04. [Tort and Hajjar 2004] recommended that \hat{D} smaller than 0.8 corresponds to the Immediate Occupancy performance level while \hat{D} values from 0.8 to 1.5 represent Life Safety performance level. Therefore, the RCFT columns of the structure are either in the Life Safety or Immediate Occupancy Performance level, indicating that the RCFT columns behaved satisfactorily. Figure 7 illustrates the damage distribution over the material fibers at a typical RCFT cross-section located in the first story of the frame. The damage levels were detected based on the material constitutive relations of the steel and concrete fibers. It can be seen that the majority of the fibers experienced steel yielding and concrete cracking. However, the high damage levels of concrete crushing and local buckling were not distributed significantly over the cross-section, indicating the good performance of the RCFT frame consistent with its performance evaluations based on the associated damage function equations.

CONCLUSION

A mixed finite element formulation for RCFT beam-columns in composite frames was shown to be an efficient computational approach to simulate the nonlinear response of RCFT columns. The formulation was successful in estimating the nonlinear curvature fields with strong accuracy using a coarse mesh (one to four elements per member) as compared to more common displacement-based formulations. The constitutive relations accounted accurately for the key composite characteristics observed for RCFT members in the experiments. The mixed finite element formulation was also successfully used for performance-based design and demand assessment of composite RCFT structures.

ACKNOWLEDGEMENT

This work was supported by the National Science Foundation under Grant No. CMS-0084848 and by the University of Minnesota. Supercomputing resources were provided by the Minnesota Supercomputing Institute. The authors would like to thank Mr. Matthew Parkolap for his assistance with this research, Drs. Douglas Goode, Roberto Leon, Amit Varma, Shosuke Morino, and Jun Kawaguchi for providing experimental data, Drs. Donald White and Bulent Nedim Alemdar for providing the details of their computational studies, and Dr. Frank McKenna for his assistance with OpenSEES software development. Any opinions, findings, and conclusions or recommendations expressed in this material are those of the authors and do not necessarily reflect the views of the sponsors.

Table 1. Seismic Response Parameters

Response Parameter	μ (max)	$\mu + \sigma$ (max)	μ (min)	$\mu + \sigma$ (min)
Δ_r / h_r	1.18	1.30	-1.03	-0.90
IDR	1.06	1.19	-1.28	-1.11
V_s	3560	3818	-3841	-3624

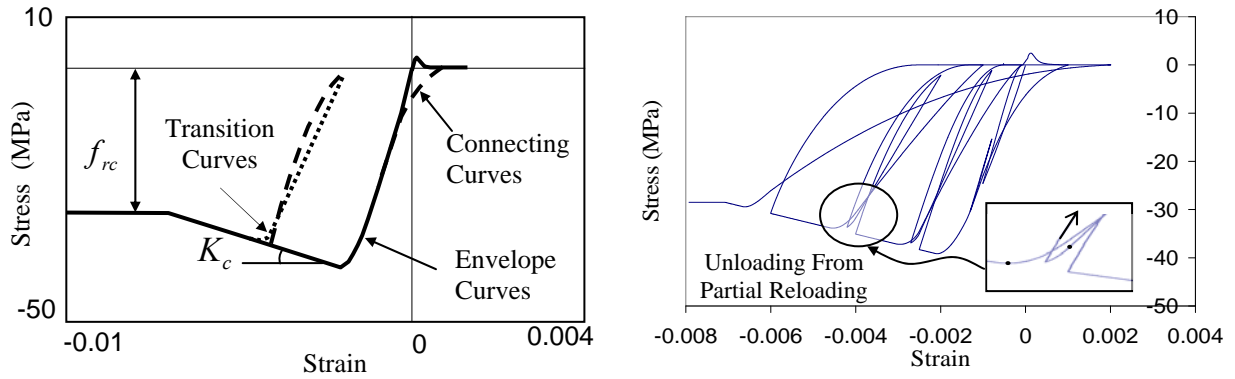


Fig. 1– Stress-Strain Response of the Concrete

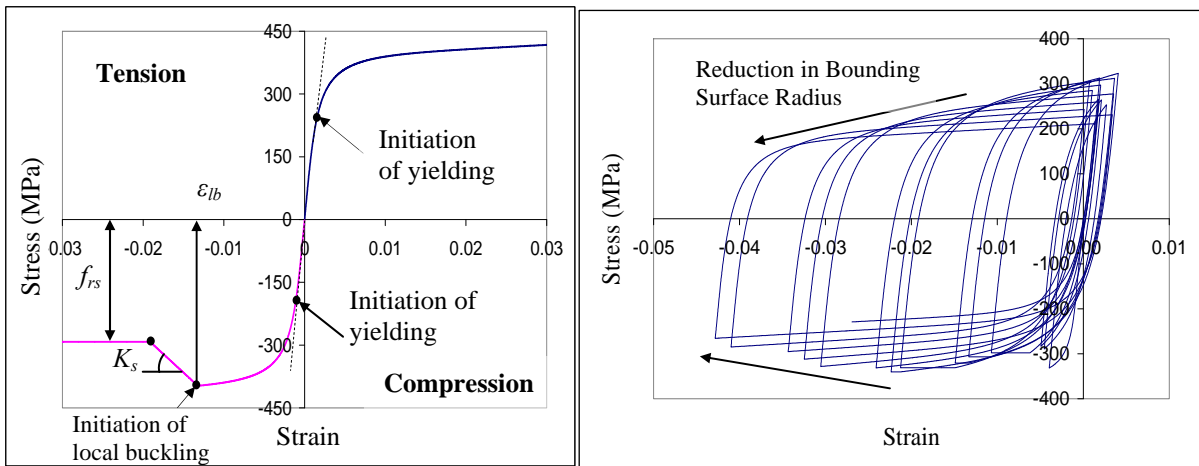


Fig. 2– Stress-Strain Response of the Steel Tube

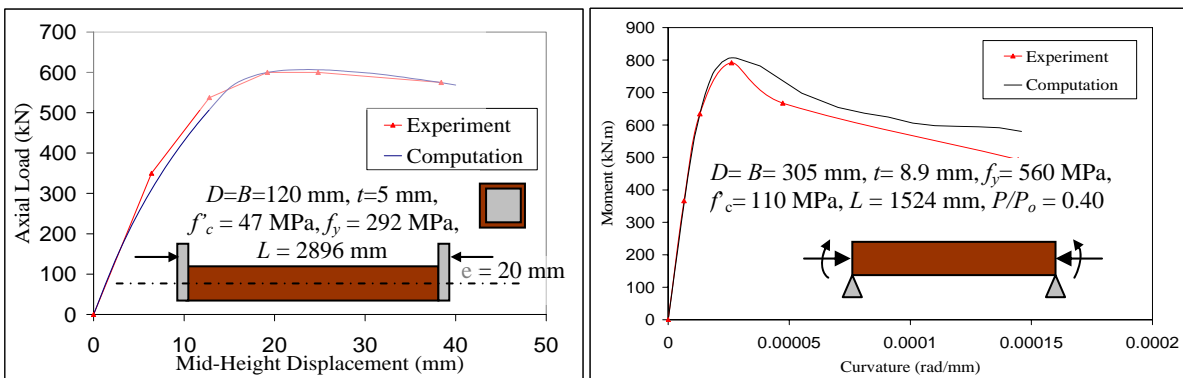


Fig. 3– Comparison of Computational and Experimental Results for RCFT Beam-Columns Specimen 1 [Cederwall et al. 1991], BC32-80-40 [Varma et al. 2002],

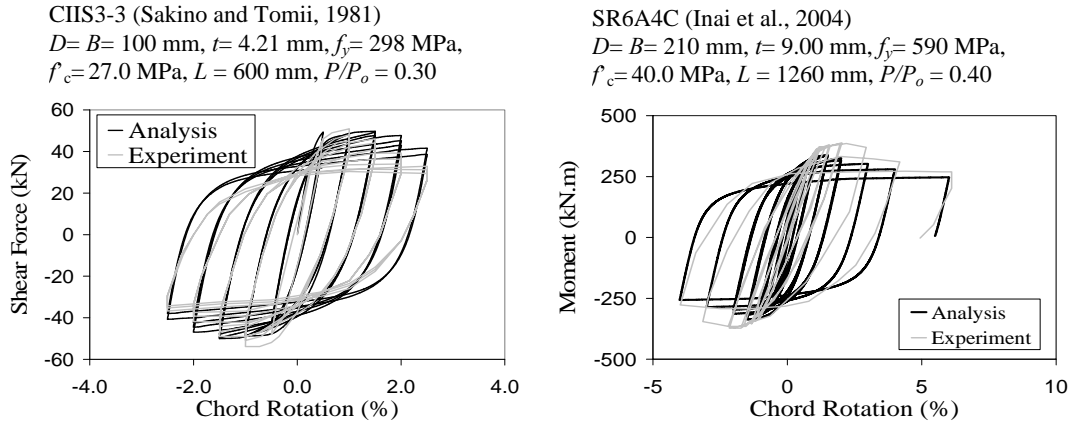


Fig. 4-Comparison of Computational and Experimental Results for Cyclically-Loaded RCFT Beam-Columns CIIS3-3 [Sakino and Tomii 1981], SR6A4C [Inai et al. 2004]

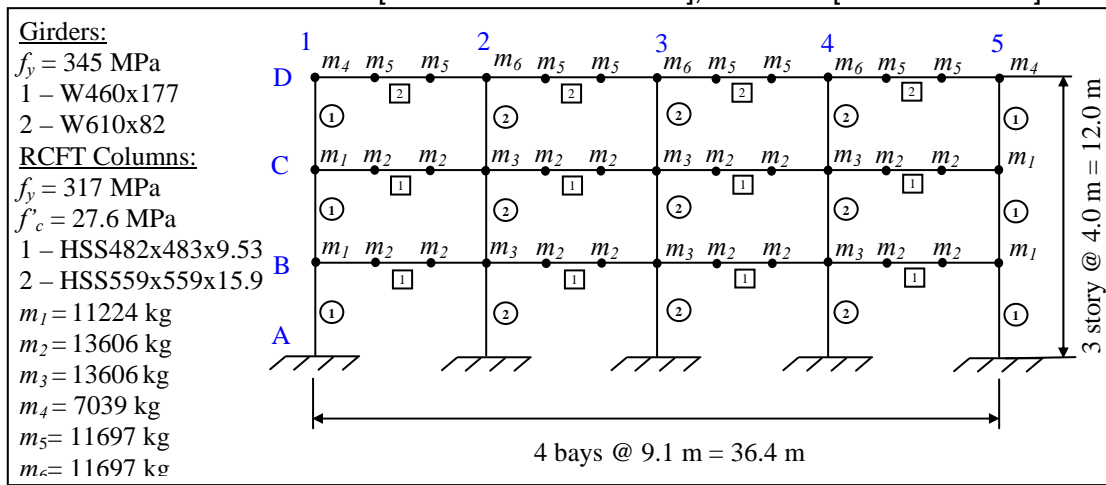


Fig. 5-RCFT Frame Configuration [LaFore and Hajjar 2005]

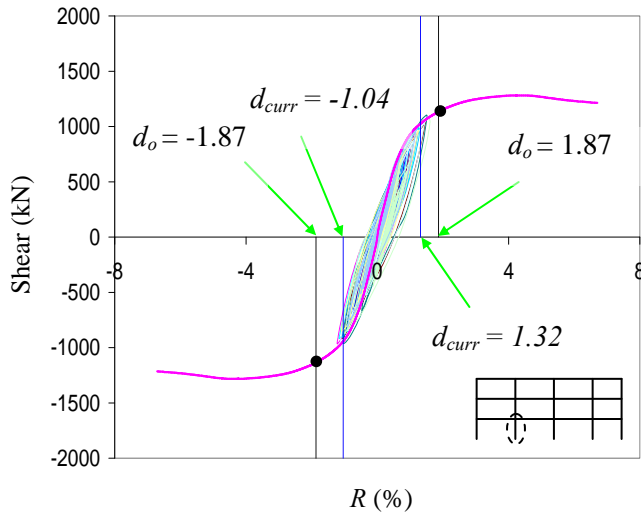


Fig. 6-Damage Function Calculation Based on Time-History Analysis

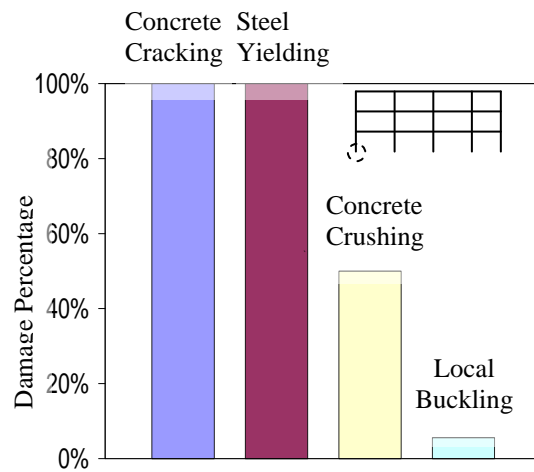


Fig. 7 - Damage Distribution at a Typical RCFT Cross-Section

NOTATION

B – width of the steel tube

C – consistent damping matrix

\hat{d} – cross-section strains from interpolation of corotational nodal displacements

d – cross-section strains corresponding to the cross-section forces

d_{curr} – the deflection of the structural member at the point in the loading history at which damage is being assessed

d_o – deflection attained when peak load is reached

\hat{d}_{sc} – slip layer deformation

D – depth of the steel tube

\hat{D} – deformation-based damage function

D – cross-section forces from interpolation corotational nodal forces

D_{Σ} – cross-section forces from numerical integration of material fiber stresses over the cross-sections

D_{sc} – force transferred between steel tube and concrete core per unit area

dx – infinitesimal length of the finite element

E_s – modulus of elasticity of the steel tube

f_y – yield strength of the steel tube

f'_c – compressive strength of concrete

f_{rc} – stress level at the constant stress region of the concrete model

f_{rs} – stress level at the constant stress region of the steel model

h_r – roof height of the building

IDR – interstory drift ratio

L – length of the RCFT member

t – thickness of the steel tube

u^c – displacement field of the concrete core

u^s – displacement field of the steel tube

\dot{u}^c – velocity field of the concrete core

\dot{u}^s – velocity field of the steel tube

\ddot{u}^c – acceleration field of the concrete core

\ddot{u}^s – acceleration field of the steel tube

q – nodal displacements

Q_{ext} – nodal forces

P – axial load

P_o – cross-section strength of RCFT cross-section

R – chord rotation

V^c – volume of the concrete core

V^s – volume of the steel tube

V_s – base shear

W^p – the plastic work done
 ε_{lbf} – the strain level at initiation of local buckling
 Δ_r – roof drift
 ρ^c – unit weight of the concrete core
 ρ^s – unit weight of the steel tube
 μ – mean
 μ^c – viscosity parameter of the concrete core
 μ^s – viscosity parameter of the steel tube
 γ_{cc} – rate of reduction of the radius of the bounding surface
 $\bar{\kappa}$ – bounding surface radius
 $\bar{\kappa}_o$ – initial bounding surface radius

REFERENCES

- Aho, M. and Leon, R. T. (1997). "A Database for Encased and Concrete-Filled Columns," Report No. 97-01, School of Civil and Environmental Engineering, Georgia Institute of Technology, Atlanta, Georgia.
- Alemdar, B. N. and White, D. W. (2005). "Displacement, Flexibility, and Mixed Beam-Column Finite Element Formulations for Distributed Plasticity Analysis," *Journal of Structural Engineering*, ASCE, Vol. 131, No. 12, pp. 1811-1819.
- American Institute of Steel Construction (AISC) (2005). *Specification for Structural Steel Buildings*, AISC, Chicago, IL.
- Cederwall, K., Engstrom, B., and Grauers, M. (1990). "High-Strength Concrete Used in Composite Columns," Second International Symposium on Utilization of High Strength Concrete, W. T. (ed.), Berkeley, California, May 1990, pp. 195-214.
- Chang, G. A. and Mander, J. B. (1994). "Seismic Energy Based Fatigue Damage Analysis of Bridge Columns: Part I – Evaluation of Seismic Capacity," Report No. NCEER-94-0006, National Center for Earthquake Engineering Research, State University of New York, Buffalo, New York.
- Choi, Y. H., Foutch, D. A., LaFave, J. M. (2006). "New Approach to AISC P–M Interaction Curve for Square Concrete Filled Tube (CFT) Beam–Columns," *Engineering Structures*, Vol. 28, No. 11, pp. 1586-1598.
- Gourley, B. C., Tort, C., Denavit, M. D., Schiller, P. H., and Hajjar, J. F. (2008). "A Synopsis of Studies of the Monotonic and Cyclic Behavior of Concrete-Filled Steel Tube Beam-Columns," Report No. UILU-ENG-2008-1802, Newmark Structural Laboratory Report Series (ISSN 1940-9826), Department of Civil and Environmental Engineering, University of Illinois at Urbana-Champaign, Urbana, Illinois, April.
- Hajjar, J. F., Schiller, P. H., and Molodan, A. (1998). "A Distributed Plasticity Model for Concrete-Filled Steel Tube Beam-Columns with Interlayer Slip," *Engineering Structures*, Vol. 20, No. 8, pp. 663-676.
- Herrera, R. (2005). "Seismic Behavior of Concrete-Filled Tube Column-Wide Flange Beam Frames," Ph.D. dissertation, Department of Civil and Environmental Engineering, Lehigh University, Bethlehem, Pennsylvania, September.

- Inai, E., Mukai, A., Kai, M., Tokinoya, H., Fukumoto, T., and Mori, K. (2004). "Behavior of Concrete-Filled Tube Beam-Columns," *Journal of Structural Engineering*, Vol. 130, No. 2, pp. 189-202.
- Kim, D.K. (2005), "A Database for Composite Columns," M.S. Thesis, Graduate School, The Georgia Institute of Technology, Atlanta, Georgia.
- LaFore, S. and Hajjar, J. F. (2005). "Design of Concrete-Filled Steel Tube Frames for Assessment Under Seismic Loading," Report No. ST-05-1, Department of Civil Engineering, University of Minnesota, Minneapolis, Minnesota, May.
- Leon, R. T., Kim, D. K., and Hajjar, J. F. (2007), "Limit State Response of Composite Columns and Beam-Columns Part 1: Formulation of Design Provisions for the 2005 AISC Specification," *Engineering Journal*, AISC, Vol. 44, No. 4, Fourth Quarter, pp. 341-358.
- Mizuno, E., Shen, C., Tanaka, Y., and Usami, T. (1991). "A Uniaxial Stress-Strain Model for Structural Steels under Cyclic Loading," *Stability and Ductility of Steel Structures Steels under Cyclic Loading*, Fukumoto, Y. and Lee, G. C. (eds.), CRC Press, Boca Raton, Florida, pp. 37-48.
- OpenSEES (2001). "Open System for Earthquake Engineering Simulation," Pacific Earthquake Engineering Research Center, University of California at Berkeley, Berkeley, California.
- Sakino, K. and Tomii, M. (1981). "Hysteretic Behavior of Concrete Filled Square Steel Tubular Beam-Columns Failed in Flexure," *Transactions of the Japan Concrete Institute*, Vol. 3, pp. 439-446.
- Schiller, P. H. and Hajjar, J. F. (1998). "A Distributed Plasticity Formulation for Three-Dimensional Rectangular Concrete-Filled Steel Tube Beam-Columns and Composite Frames," Report No. ST-96-5, Department of Civil Engineering, University of Minnesota, Minneapolis, Minnesota.
- Tort, C. and Hajjar, J. F. (2004). "Damage Assessment of Rectangular Concrete-Filled Steel Tubes for Performance-Based Design," *Earthquake Spectra*, Vol. 20, No. 4, pp. 1317-1348.
- Tort, C. and Hajjar, J. F. (2007). "Reliability-Based Performance-Based Design of Rectangular Concrete-Filled Steel Tube (RCFT) Members and Frames," Report No. ST-07-1, Department of Civil Engineering, University of Minnesota, Minneapolis, Minnesota.
- Tsai, K. C., Weng, Y., Lin, M., Chen, C., Lai, J., and Hsiao, P. (2003). "Pseudo Dynamic Tests of a Full-Scale CFT/BRB Composite Frame: Displacement Based Seismic Design and Response Evaluations," International Workshop on Steel and Concrete Composite Construction (IWSCCC-2003), National Center for Research on Earthquake Engineering, Taipei, Taiwan, October 8-9, 2003, National Center for Research on Earthquake Engineering, Taipei, Taiwan, pp. 165-176.
- Varma, A. H., Ricles, J. M., Sause, R., and Le-Wu, L. (2002). "Experimental Behavior of High Strength Square Concrete-Filled Steel Tube Beam-Columns," *Journal of Structural Engineering*, ASCE, Vol. 128, No. 3, pp. 309-318.
- Yun, S., Hamburger, R. O., Cornell, C. A., and Foutch, D. A. (2002). "Seismic Performance Evaluation for Steel Moment Frames," *Journal of Structural Engineering*, ASCE, Vol. 128, No. 4, pp. 534-545.